Journal of Molecular Catalysis A: Chemical 353–354 (2012) 58–66

Contents lists available at SciVerse ScienceDirect

Journal of Molecular Catalysis A: Chemical

journal homepage: www.elsevier.com/locate/molcata

The effect of Cu loading on the formation of methyl formate and C_2-oxygenates from CH_3OH and CO over K- or Cs-promoted Cu-MgO catalysts

Shahin Goodarznia, Kevin J. Smith*

Department of Chemical and Biological Engineering, The University of British Columbia, 2360, East Mall, Vancouver, BC, Canada, V6T 1Z3

ARTICLE INFO

Article history:
Received 26 July 2011
Received in revised form 21 October 2011
Accepted 1 November 2011
Available online 11 November 2011

Keywords:
Catalyst
Promoter
Synthesis gas
Methyl formate
Methanol
Ethanol
Copper
Magnesium oxide
Dispersion
Basicity

ABSTRACT

The reaction of CH_3OH in the presence of CO at 101 kPa over K- or Cs-promoted Cu-MgO is reported. The selectivity to methyl formate was >92 C-atom% whereas selectivity to CO_2 and C_2 species (ethanol and acetic acid) was <8 C-atom% at 498 and 523 K over the promoted 5 wt% Cu-MgO catalyst. The activity increased as the Cu loading was increased from 5 wt% to 40 wt%, whereas at the same conversion, the product distribution was almost the same over both the 0.5 wt% Cs–5 wt% Cu-MgO and the 0.5 wt% Cs–40 wt% Cu-MgO catalysts. At approximately constant specific basicity, an increase in Cu^0 surface area of the promoted Cu-MgO catalysts correlated with an increased methyl formate yield, whereas no correlation between Cu^{2+} surface area and methyl formate yield was observed. The results suggest that methyl formate is formed on Cu^0 sites as opposed to Cu^{2+} sites. The mechanism of methyl formate formation from CH_3OH over the promoted Cu-MgO catalysts is discussed in view of these results.

1. Introduction

Ethanol as an additive to gasoline (fuel ethanol) has received significant attention in past decades due to the environmental impact of fossil fuels such as gasoline. In 2005, the addition of fuel ethanol to gasoline displaced 2% of the world-wide annual consumption of gasoline and this value is anticipated to increase to 10% by 2030 [1]. Using conventional methods to produce this amount of ethanol will result in a shortage of approximately 262 gl of fuel ethanol by 2030 [1]. The expected rapid increase in worldwide consumption of fuel ethanol requires an increase in worldwide ethanol production. Most of the world's ethanol is produced by fermentation using biomass as a main source of carbon. The process is expensive and energy inefficient due to intensive distillation steps [2,3]. Furthermore, the fermentation process does not utilize all the carbon available in the biomass, which results in low yields of ethanol. An alternative approach, which has significant potential to reduce greenhouse gas emissions associated with fossil fuels, is the selective conversion of biomass-derived syngas ($CO/CO_2/H_2$) to ethanol.

The synthesis of CH_3OH from syngas over Cu-ZnO based catalyst is very well known [4–12]. Addition of alkali promoters (K or Cs) to Cu-ZnO catalysts shifts the conversion of syngas away from CH_3OH and towards heavier alcohols such as iso-butanol, but the selectivity to ethanol remains low [13–16]. Mechanistic studies of the synthesis of ethanol from syngas over Cu-ZnO-based catalysts, suggest that the presence of Cu and basic sites (i.e. ZnO) are essential to facilitate the formation of the first C–C bond [13,17–22].

Cu-MgO has been shown to be >10×'s more basic than a conventional Cu-ZnO catalyst [23,24]. In previous work, the present authors studied a series of alkali-promoted 40 wt% Cu-MgO catalysts, focusing on the effect of basicity [23]. The activity of these catalysts for methanol decomposition and C–C bond formation at low pressure (101 kPa) was reported. The formation of methyl formate over alkali-promoted 40 wt% Cu-MgO was also studied [23] as this product has been identified as an important intermediate in ethanol formation from syngas and CH_3OH [13,20]. The results of this study showed that at a relatively constant Cu^0 surface area (0.50–0.76 $m^2\,g^{-1}$), the alkali-promoted Cu-MgO had an optimum intrinsic basicity (9.5 $\mu mol\,CO_2\,m^{-2}$) at which the selectivity to methyl formate and C_2 species (ethanol and acetic acid) was maximized [23]. The selectivity to methyl formate was found to be very sensitive to the intrinsic basicity of the alkali promoted Cu-MgO catalyst [23].

Cu sites are well known for their hydrogenating–dehydrogenating properties [25] and the presence of Cu sites in Cu-ZnO catalysts was found to facilitate CH_3OH dehydrocoupling to methyl

* Corresponding author. Tel.: +1 604 822 3601; fax: +1 604 822 6003.
E-mail address: kjs@interchange.ubc.ca (K.J. Smith).

1381-1169/$ – see front matter © 2011 Elsevier B.V. All rights reserved.
doi:10.1016/j.molcata.2011.11.005

formate [26,27]. Based on previous mechanistic studies over mainly Cu-ZnO based catalysts and Cu-MgO-based catalysts [13,17–23], it is apparent that the state of surface Cu (Cu^0 or Cu^{2+}) is an important variable in determining the catalyst selectivity to higher alcohols, such as ethanol.

In the present study, the effect of the Cu oxidation state and the Cu surface area on the activity of a series of alkali-promoted Cu-MgO catalysts of approximately constant basicity, is reported. The formation of C_2 species and methyl formate from CH_3OH/CO at 101 kPa is reported over high surface area 5 wt% Cu-MgO catalysts, promoted with K and Cs, prepared using the method described previously [23,28] and characterized to quantify the surface Cu^0 and basic sites. The results have been compared with data reported previously for alkali-promoted 40 wt% Cu-MgO catalysts with relatively low Cu dispersions [23].

Note that the synthesis of alcohols from syngas is usually done at high pressures (>5 MPa) to overcome thermodynamic yield limitations of the methanol synthesis [15,21,25]. The higher alcohols are favoured by thermodynamics at these conditions. The use of low pressure (101 kPa) in the present study simplifies the experimental procedure. Also, using CH_3OH as reactant and operating at 101 kPa, leads to the decomposition of CH_3OH that likely generates carbonaceous surface species such as formyl, formate and methoxy species that can react further to produce methyl formate or C_2 species.

2. Experimental

2.1. Catalyst preparation

High surface area 5 wt% Cu-MgO and alkali promoted 5 wt% Cu-MgO (0.5 wt% K–5 wt% Cu-MgO and 0.5 wt% Cs–5 wt% Cu-MgO) were prepared by thermal decomposition of metal salts ($Mg(NO_3)_2{\cdot}6H_2O$, $Cu(NO_3)_2{\cdot}3H_2O$, Cs_2CO_3 and KNO_3) in the presence of palmitic acid ($CH_3(CH_2)_{14}COOH$). The details of the catalyst preparation procedure have been reported previously [23]. Note that the final calcination temperature used for each catalyst precursor was determined by the highest decomposition temperature of the metal nitrates or carbonates present in the precursor and as a result, the calcination temperature for the 5 wt% Cu-MgO, 0.5 wt% K–5 wt% Cu-MgO and 0.5 wt% Cs–5 wt% Cu-MgO were respectively 673 K, 873 K and 923 K. Following calcination, the catalyst precursors were reduced by heating to 573 K at a rate of 10 K min^{-1} in 10% H_2/He, with the final temperature held for 60 min.

2.2. Catalyst characterization

Temperature-programmed reduction (TPR) of the prepared catalyst precursors was performed using a Micromeritics AutoChem II chemisorption analyzer, with a 10% H_2/Ar gas flow of 50 cm^3(STP) min^{-1} while heating from 313 K to 623 K at a ramp rate of 10 K min^{-1}, with the final temperature held for 30 min. Prior to the TPR, samples (about 0.2 g) were pre-treated thermally in He at 50 cm^3(STP) min^{-1} and 393 K. The TPR profiles of the 5 wt% Cu-MgO-based catalysts of the present study were compared to the TPR profiles of CuO and Cu_2O (97% purity, particle size < 5 μm, Sigma–Aldrich) reported previously [23].

Catalyst BET surface areas, pore volume, pore diameter and pore size distribution of the calcined 5 wt% Cu-MgO catalyst precursors were measured using a Micromeritics ASAP 2020 analyzer [23]. Catalyst BET surface area of the reduced 5 wt% Cu-MgO-based catalysts were measured using Micromeritics AutoChem II chemisorption analyzer [23]. Basic properties of the reduced catalysts were determined by CO_2 temperature-programmed desorption (TPD) using a Micromeritics AutoChem II chemisorption analyzer, details of which are provided elsewhere [23].

Table 1
Cu-MgO-based catalyst nominal name and composition.

Catalyst nominal name	Catalyst composition (wt%)			
	Cu	MgO	K	Cs
40 wt% Cu-MgO[a]	40.3	59.3	0	0
0.5 wt% K–40 wt% Cu-MgO[a]	40.1	59.4	0.5	0
0.5 wt% Cs–40 wt% Cu-MgO[a]	40.1	59.4	0	0.5
5 wt% Cu-MgO	5.0	95.0	0	0
0.5 wt% K–5 wt% Cu-MgO	5.0	94.5	0.5	0
0.5 wt% Cs–5 wt% Cu-MgO	5.0	94.5	0	0.5

[a] Catalysts reported previously [23].

X-ray powder diffraction (XRD) patterns of the calcined catalyst precursors were obtained with a Rigaku Multiflex diffractometer using Cu Kα radiation (λ = 0.154 nm, 40 kV and 20 mA), a scan range of 2θ from 10° to 100° and a step size of 2° min^{-1} [23]. The MgO crystallite size (d^{XRD}_{MgO}) was determined from the XRD data using the Scherrer equation [23]. The Cu crystallite size (d^{XRD}_{Cu}) was estimated from the CuO crystallite size of the calcined samples, corrected for the differences in molar volume between the CuO and the Cu [23]. The Cu dispersion and Cu surface area of the reduced 5 wt% Cu-MgO-based catalysts were measured by adsorption and decomposition of N_2O on the Cu surface using a Micromeritics AutoChem II chemisorption analyzer [23].

X-ray photoelectron spectroscopy (XPS) studies of the passivated, reduced catalysts, were conducted using a Leybold Max200 X-ray photoelectron spectrometer. Al Kα was used as the photon source generated at 15 kV and 20 mA. The pass energy was set at 192 eV for the survey scan and 48 eV for the narrow scan. The reduced Cu-MgO-based catalyst with Cu content of 34.6–40.1 wt% was passivated in a flow of 100 cm^3(STP) min^{-1} of 1% O_2/He for 120 min. All XPS spectra were corrected to the Mg 2p peak at 50.8 eV.

2.3. Catalyst testing

Catalyst testing was conducted in a plug flow micro-reactor, details of which have been reported previously [23]. Note that for all of the reaction experiments, 0.98 g of catalyst was used with a reactant mixture of CO/He/CH_3OH (0.20/0.66/0.14 M). In each test, net conversion was defined as the total C-atom conversion of [CH_3OH + CO] and is the sum of the net CO consumption and the net CH_3OH conversion. In all cases net CO consumption was in the range of 3–10 C-atom %, implying that the rate of CH_3OH decomposition to CO was lower than the rate of CO conversion to different carbonaceous products. Therefore the net CO yield and selectivity in the product stream were assumed to be zero. The product yield was calculated as the product of the total exit molar flow rate and the component mole fraction divided by total exit molar flow rate, excluding He. Component selectivity was determined as the total C-atom conversion divided by the product yield.

3. Results and discussion

3.1. Catalyst characterization

The nominal composition of the catalysts discussed in the present study is reported in Table 1. The catalyst BET surface area (S_{BET}), pore volume (V_p) and average pore diameter (d_p) of the 5 wt% Cu-MgO-based catalysts are compared to the 40 wt% Cu-MgO-based catalysts [23] in Table 2. For the 5 wt% Cu-MgO-based catalysts, d_p was in the range 14–26 nm, indicative of a mesoporous catalyst. For the 5 wt% Cu-MgO-based catalysts, the S_{BET}

Table 2
BET surface area, pore volume and pore size of alkali promoted Cu-MgO catalysts.

Catalyst	S_{BET}[a] ($m^2\ g^{-1}$)		V_p[a] ($cm^3\ g^{-1}$)	d_p[a] (nm)
	After calcination	After reduction		
MgO[b]	160	160	0.58	14.5
40 wt% Cu-MgO[b]	62	74	0.23	15.0
0.5 wt% K–40 wt% Cu-MgO[b]	35	42	0.20	23.1
0.5 wt% Cs–40 wt% Cu-MgO[b]	38	44	0.20	20.8
5 wt% Cu-MgO	141	141	0.49	14.0
0.5 wt% K–5 wt% Cu-MgO	60	60	0.37	24.5
0.5 wt% Cs–5 wt% Cu-MgO	51	51	0.33	26.0

[a] S_{BET} is the BET surface area; V_p and d_p are respectively, the pore volume and average pore size of the calcined catalyst precursor.
[b] Characterization data taken from [23].

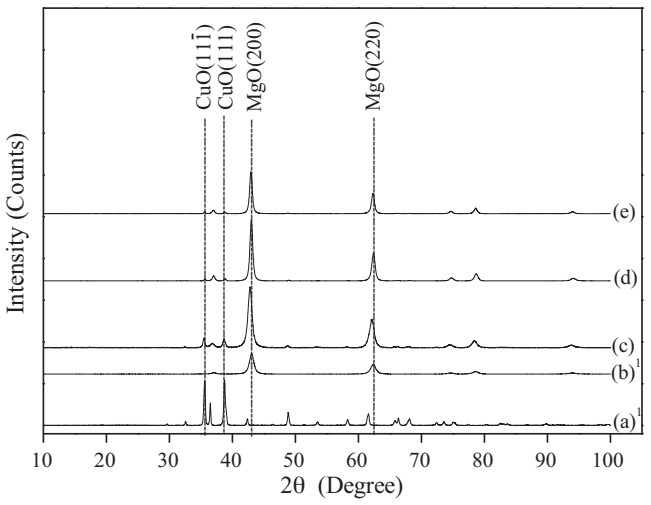

Fig. 2. X-ray diffractograms of the unreduced MgO-based catalysts and bulk CuO: (a) CuO; (b) MgO; (c) 5 wt% Cu-MgO; (d) 0.5 wt% K–5 wt% Cu-MgO; (e) 0.5 wt% Cs–5 wt% Cu-MgO.
[1] Data from [23].

remained unchanged after reduction compared to the S_{BET} after calcination (Table 2). Since the catalyst Cu loading was low, only small amounts of water were generated during reduction of CuO to Cu. Consequently, there was a negligible change in porosity and S_{BET} following reduction.

The pore size distributions of the calcined 5 wt% Cu-MgO-based catalyst precursors are compared to those of the 40 wt% Cu-MgO-based catalysts and MgO in Fig. 1. Compared to MgO, the addition of 5 wt% Cu shifted the maxima of the pore size distribution to a higher pore diameter, whereas both the S_{BET} and V_p decreased (Table 2). These observations are in good agreement with the trend reported previously for the 40 wt% Cu-MgO-based catalysts [23]. Comparison of the pore size distribution of the 5 wt% Cu-MgO and 40 wt% Cu-MgO (Fig. 1), showed that an increase in Cu loading broadened the catalyst pore size distribution and led to a decrease in S_{BET} and V_p of the Cu-MgO (Table 2). These observations imply that an increase in Cu loading most likely led to blockage of the small pores (d_p < 10 nm) of MgO by CuO.

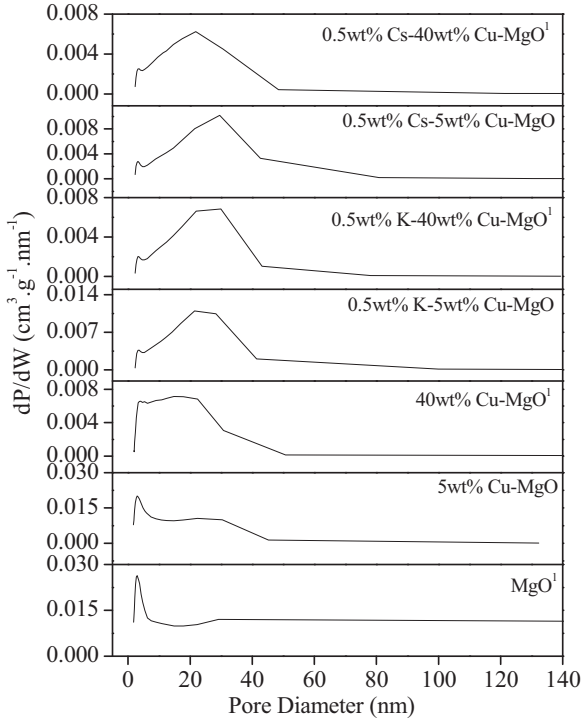

Fig. 1. Pore size distribution of MgO, unreduced 5 wt% Cu-MgO-based catalysts and unreduced 40 wt% Cu-MgO-based catalyst.
[1] Data was taken from the previous study [23].

Addition of 0.5 wt% Cs or 0.5 wt% K to the 5 wt% Cu-MgO decreased the S_{BET} and V_p (Table 2), as was similarly observed with the addition of 0.5 wt% Cs or 0.5 wt% K to 40 wt% Cu-MgO [23]. Previously, it was shown that a decrease in S_{BET} and V_p after addition of Cs or K to the Cu-MgO was caused by (1) thermal sintering of the catalyst due to the higher calcination temperature of the alkali promoted Cu-MgO compared to the Cu-MgO and (2) pore blocking of MgO by K promoter or Cs promoter [23]. In the present study, the same effects of promoters and caclination temperature are apparent from the shift in the maxima of the pore size distribution to higher pore diameter after addition of 0.5 wt% Cs or 0.5 wt% K to 5 wt% Cu-MgO (Fig. 1).

Comparing the pore size distribution (Fig. 1) of the 0.5 wt% K–5 wt% Cu-MgO and the 0.5 wt% K–40 wt% Cu-MgO, reveals almost the same pore size distribution for both catalysts. The same trend was observed for the 0.5 wt% Cs–5 wt% Cu-MgO and the 0.5 wt% Cs–40 wt% Cu-MgO (Fig. 1). These observations show that an increase in Cu loading from 5 wt% to 40 wt% of the K- or Cs-promoted Cu-MgO does not affect the catalyst pore size distribution noticeably, implying that high temperature thermal sintering and the presence of the alkali promoters are the major factors determining the pore size distribution of the K- or Cs-promoted Cu-MgO.

The X-ray diffractogram of the calcined 5 wt% Cu-MgO catalyst precursors (Fig. 2) showed the presence of MgO (periclase, *Fm*3*m*(225)-cubic structure) and CuO (tenorite, *C*2/*c*(15) monoclinic structure). No peaks associated with Cu_2O, K_2O or Cs_2O were detected. The observations are in good agreement with the XRD analysis of the 40 wt% Cu-MgO-based catalysts [23]. Note that the X-ray diffractograms of CuO and MgO [23], are included in Fig. 2 for comparison purposes. Using the data of Fig. 2, the MgO crystallite thickness (d^{XRD}_{MgO}) and the Cu crystallite thickness (d^{XRD}_{Cu}) were estimated and the results are reported in Table 3. For the 5 wt% Cu-MgO-based catalysts, d^{XRD}_{MgO} and d^{XRD}_{Cu} increased as the S_{BET} and V_p decreased, supporting the assertion that the loss in S_{BET} and V_p was partly due to thermal sintering of the Cu and MgO crystallites and in agreement with the results from the 40 wt% Cu-MgO catalysts [23]. The data of Table 3 also show that a decrease in Cu loading from 40 wt% to 5 wt% led to almost no change in d^{XRD}_{MgO} and d^{XRD}_{Cu} for both the un-promoted and alkali-promoted catalysts.

Table 3
Copper dispersion, crystallite size and MgO unit cell size of 5 wt% Cu-MgO-based catalysts.

Catalyst	Cu dispersion (%)	S_{Cu^0} ($m^2\ g^{-1}$)[a]	$d_{Cu}^{N_2O}$ (nm)	d_{Cu}^{XRD} (nm)	d_{MgO}^{XRD} (nm)	a_{MgO} (nm)
MgO[b]	–	–	–	–	13	0.42
40 wt% Cu-MgO[b]	1.54	2.64	65	15	17	0.42
0.5 wt% K–40 wt% Cu-MgO[b]	0.19	0.50	519	21	20	0.42
0.5 wt% Cs–40 wt% Cu-MgO[b]	0.28	0.58	362	24	20	0.42
5 wt% Cu-MgO	13.52	1.24	8	17	15	0.42
0.5 wt% K–5 wt% Cu-MgO	2.98	0.26	34	21	19	0.42
0.5 wt% Cs–5 wt% Cu-MgO	13.24	1.10	8	26	20	0.42

[a] Copper metal surface area was calculated assuming 1.46×10^{19} copper atoms per m^2.
[b] Data reported in [23].

The XRD data were used to calculate the unit cell size of the MgO (a_{MgO}) as reported in Table 3. The results show that a_{MgO} remained unchanged with the addition of the CuO as well as the K promoter or Cs promoter to the 5 wt% Cu-MgO, implying that there was no solid solution present in the catalyst. Similar observations were made for the 40 wt% Cu-MgO catalysts, suggesting that the preparation of the unreduced Cu-MgO-based catalysts using palmitic acid yields separate phases of MgO, CuO and alkali promoters (K or Cs), rather than solid solutions.

The Cu dispersion of the 5 wt% Cu-MgO-based catalysts was measured by N_2O adsorption–decomposition and the results, reported in Table 3, show that the Cu dispersion varied from 2% to 13%. Addition of K to the 5 wt% Cu-MgO catalyst led to a decrease in Cu dispersion, similar to the results obtained for the 40 wt% Cu-MgO catalysts [23]. We assume that K_2O (or KOH) readily wets the Cu, which leads to a decrease in Cu dispersion. Addition of Cs to the 5 wt% Cu-MgO catalyst did not affect the Cu dispersion significantly, whereas addition of Cs to the 40 wt% Cu-MgO decreased the Cu dispersion (Table 3). These results suggest a strong interaction between the Cs_2O and the MgO that prevents the Cs_2O from wetting the Cu. However at high Cu loading some interaction between the Cs and the Cu must occur which leads to a decrease in Cu dispersion. Comparing the Cu dispersion of the 5 wt% Cu-MgO-based catalysts (Table 3) with the 40 wt% Cu-MgO-based catalysts (Table 3) shows that a decrease in Cu loading improved the Cu dispersion. The Cu crystallite size of the 5 wt% Cu-MgO catalysts measured by N_2O adsorption–decomposition ($d_{Cu}^{N_2O}$) as well as by XRD (d_{Cu}^{XRD}) is shown in Table 3. Both $d_{Cu}^{N_2O}$ and d_{Cu}^{XRD} are in good agreement for all of the 5 wt% Cu-MgO-based catalysts, implying that the Cu crystallites (diameter < 30 nm) were not occluded from the surface and are well dispersed. On the other hand, the 40 wt% Cu-MgO-based catalysts had low Cu dispersion and a significant difference between the $d_{Cu}^{N_2O}$ and d_{Cu}^{XRD} values, suggesting that the Cu was occluded from the surface of the 40 wt% Cu-MgO-based catalysts [23]. Clearly, a decrease in Cu loading from 40 wt% to 5 wt%, led to an increase in Cu dispersion.

The TPR profiles of the calcined catalyst precursors of the present study are shown in Fig. 3 and the reduction peak temperatures and calculated degrees of reduction are summarized in Table 4. For comparison, the TPR profiles of CuO and Cu_2O [23] are also reported in Fig. 3 and Table 4. The TPR curve for bulk CuO was deconvoluted to show a reduction peak at 480 K and 520 K (Fig. 3). The lower peak temperature is attributed to the reduction of CuO and the higher peak temperature is likely a consequence of the reduction of large CuO particles (diameter ~ 270 μm) via shrinking core kinetics. Reduction of the bulk (unsupported) CuO is initiated on the surface so that subsequently, the sample consists of a layer of Cu^0 over a CuO core. Reduction of the core is therefore limited by H_2 diffusion to the core of large, partially reduced Cu-CuO, and this is reflected in an apparent higher reduction temperature in the TPR profile. The Cu_2O showed a reduction peak at 594 K. The TPR profiles of all the 5 wt% Cu-MgO-based catalysts (Fig. 3) show a reduction peak in the range of 479–486 K (Table 2) that can be attributed to the reduction of bulk CuO, in agreement with the XRD results (Fig. 2) that detected the presence of bulk CuO as the only reducible species in the calcined 5 wt% Cu-MgO-based catalyst. These results show that the CuO of the 5 wt% Cu-MgO-based catalysts was well dispersed, in good agreement with the high Cu dispersion of the 5 wt% Cu-MgO-based catalysts reported in Table 3, so that during reduction, H_2 diffusion into the core of the catalysts was not rate controlling. Since for all of the 5 wt% Cu-MgO catalysts reduction peaks were significantly below the Cu_2O reduction peak temperature (Table 4), it can be concluded that no Cu_2O was present in the 5 wt% Cu-MgO catalysts.

The TPR results of the 5 wt% Cu-MgO-based catalysts revealed that, in all cases, the degree of reduction of the CuO was only between 30% and 40%, likely due to the high Cu dispersion of the 5 wt% Cu-MgO-based catalysts (Table 3) and the associated strong interaction between CuO and MgO that prevented complete CuO reduction. On the other hand, previously we reported that all the 40 wt% Cu-MgO-based catalysts had >80% reduction but low Cu dispersions (0.2–1.5%) [23] which is indicative of weaker interaction

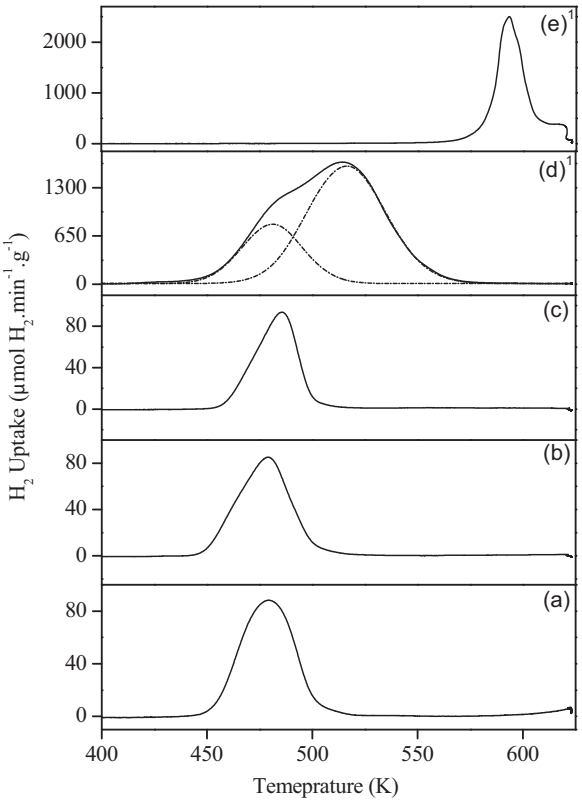

Fig. 3. Temperature program reduction profile for: (a) 5 wt% Cu-MgO; (b) 0.5 wt% K–5 wt% Cu-MgO; (c) 0.5 wt% Cs–5 wt% Cu-MgO; (d) CuO; (e) Cu_2O.
[1]Data were taken from the previous study [23].

Table 4
Temperature programmed reduction results for 5 wt% Cu-MgO-based catalysts.

Sample	Hydrogen consumption (mmol g^{-1} catalyst)	Degree of reduction (%)	Reduction peak temperature (K)
Cu_2O-reference[a]	6.84	100	594
CuO-reference[a]	11.06	88	480 and 520
5 wt% Cu-MgO	0.27	38	479
0.5 wt% K–5 wt% Cu-MgO	0.26	35	479
0.5 wt% Cs–5 wt% Cu-MgO	0.24	30	486

[a] Data reported in [23].

between CuO and MgO that resulted in higher degree of reduction. Addition of K- or Cs-promoter to the 5 wt% Cu-MgO, caused a slight decrease in the CuO degree of reduction (Table 4).

The CO_2 TPD profiles for all of the 5 wt% Cu-MgO-based catalysts are shown in Fig. 4 and the corresponding results are summarized in Table 5. For the purpose of comparison, the catalyst intrinsic basicity and distribution of basic sites for the 40 wt% Cu-MgO-based catalyst and MgO are also reported in Table 5. Addition of K or Cs to the 5 wt% Cu-MgO, increased the intrinsic basicity while the distribution of basic sites was almost unchanged (Table 5). This observation is in good agreement with the observation made for the K or Cs promoted 40 wt% Cu-MgO-based catalysts (Table 5).

Addition of 5 wt% Cu to MgO increased the intrinsic basicity but the distribution of basic sites was almost unchanged compared to the MgO. Comparing the intrinsic basicity of the 5 wt% Cu-MgO (3.9 μmol CO_2 m^{-2}) to that of the 40 wt% Cu-MgO (4.3 μmol CO_2 m^{-2}) (Table 5) shows that an increase in Cu loading from 5 wt% to 40 wt%, increased the intrinsic basicity but the distribution of basic sites remained unchanged. The same trend was observed for the 0.5 wt% K–Cu-MgO (Table 5) and for the 0.5 wt% Cs–Cu-MgO (Table 5), as the Cu loading was increased from 5 wt% to 40 wt%. Previous studies [23,29] suggested that in Cu-MgO, Cu gains a large net positive charge while the Cu electrons are transferred to MgO, which most likely leads to an increase in the oxygen partial negative charge in MgO. The results of the present study are in good agreement with this assertion. Of note is the fact that the intrinsic basicity of the 0.5 wt% K and Cs promoted Cu-MgO were in a narrow range (385–415 μmol CO_2 g^{-1}) for both the 5 wt% Cu and the 40 wt% Cu catalysts.

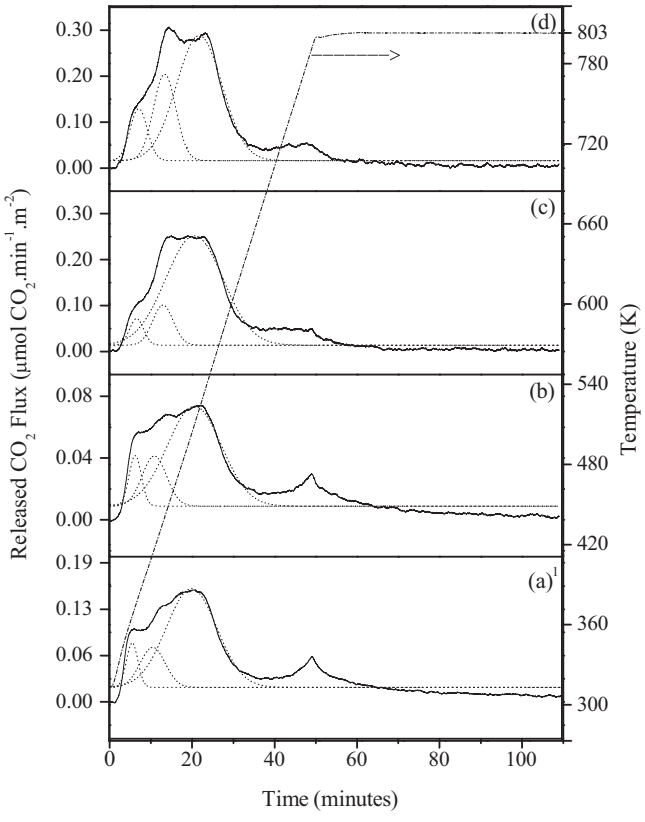

Fig. 4. CO_2 temperature program desorption of (a) MgO;(b) 5 wt% Cu-MgO; (c) 0.5 wt% K–5 wt% Cu-MgO; (d) 0.5 wt% Cs–5 wt% Cu-MgO.
[1] Data from [23].

The surface composition of the K- or Cs-promoted 40 wt% Cu-MgO catalysts, as measured by XPS, is summarized in Table 6. The Mg 2p spectra showed a binding energy of 50.86 eV (Table 6) which corresponds to Mg^{2+} in MgO [30]. The C 1s spectra showed a peak at BE 285.88 eV to 286.74 eV (Table 6) which indicates carbon contamination of the Cu-MgO-based catalyst due to MgO bonding with $HCOOCH_3$ [31] that occurs because of the presence of palmitic acid in the catalyst precursor. Note that XPS analysis conducted on the 0.5 wt% K–5 wt% Cu-MgO and the 0.5 wt% Cs–5 wt% Cu-MgO (not reported herein) showed similar Mg 2p and C 1s peaks compared to the K- or Cs-promoted-40 wt% Cu-MgO catalysts, but no peak corresponding to Cu was detected, likely due to the surface Cu concentration being lower than the detection limit of the XPS unit. For the 0.5 wt% K–40 wt% Cu-MgO and the 0.5 wt% Cs–40 wt% Cu-MgO, no XPS peaks associated with Cs or K were observed, because the alkali promoter surface concentration was below the XPS detection limit. Consequently, catalysts with higher concentrations of alkali metal were prepared for XPS analysis. Previous studies have shown that the K 2p BE of 297.3 eV is attributable to the presence of K_2O whereas a K 2p BE of 292.8–293.1 eV is attributable to the presence of KOH [32]. XPS analysis conducted on a 4.4 wt% K–40 wt% Cu-MgO catalyst showed a K 2p BE of 294.65 eV, which indicated the presence of mostly KOH. However since the K 2p BE of the present study is slightly higher than the KOH K 2p BE, the presence of small amounts of K_2O is also possible. This reveals that KNO_3 was successfully decomposed to KOH and K_2O during catalyst calcination of the 4.4 wt% K–40 wt% Cu-MgO catalyst. Results of the XPS analysis of a 13.5 wt% Cs–40 wt% Cu-MgO showed a Cs 3d BE of 725.89 eV, which reveals the presence of Cs^+ in the form of Cs_2O on the surface of the catalyst [33]. This reveals that Cs_2CO_3 was successfully decomposed to Cs_2O during catalyst calcination of the 13.5 wt% Cs–40 wt% Cu-MgO catalyst. Note that oxidation state of the promoters determined by XPS analysis of the 4.4 wt% K–40 wt% Cu-MgO and 13.5 wt% Cs–40 wt% Cu-MgO, is assumed to also be valid for the 0.5 wt% alkali promoted-40 wt% Cu-MgO catalyst, in agreement with other studies [32,33].

Cu 2p XPS spectra of the passivated K- or Cs-promoted-40 wt% Cu-MgO catalysts are shown in Fig. 5 and the corresponding Cu $2p_{1/2}$ (satellite), Cu $2p_{1/2}$ (parent), Cu $2p_{3/2}$ (satellite) and Cu $2p_{3/2}$ (parent) BEs are reported in Table 7. Based on the XPS results, all the passivated alkali promoted-40 wt% Cu-MgO catalysts showed the presence of CuO on the catalyst surface. Area ratios of the Cu $2p_{1/2}$ (satellite) and Cu $2p_{1/2}$ (parent) (Cu_s/Cu_p), indicative of the degree of Cu oxidation [34], were calculated for all the passivated K- or Cs-promoted 40 wt% Cu-MgO catalysts and are reported in Table 7. The Cu_s/Cu_p ratio of all the passivated alkali promoted-40 wt% Cu-MgO catalysts was noticeably lower than the Cu_s/Cu_p ratio in CuO

Table 5
Basic properties of MgO-based catalyst measured by means of CO_2 TPD.

Catalyst	Specific basicity (μmol CO_2 g^{-1})	Intrinsic basicity (μmol CO_2 m^{-2})	Distribution of different basic sites on the catalyst (%)		
			Weak	Medium	Strong
MgO[a]	432.0	2.7	8	15	77
40 wt% Cu-MgO[a]	315.5	4.3	9	19	72
0.5 wt% K–40 wt% Cu-MgO[a]	392.4	9.3	11	21	69
0.5 wt% Cs–40 wt% Cu-MgO[a]	415.9	9.5	16	19	65
5 wt% Cu-MgO	547.1	3.9	9	17	75
0.5 wt% K–5 wt% Cu-MgO	394.8	6.6	5	11	84
0.5 wt% Cs–5 wt% Cu-MgO	384.5	7.5	10	23	67

[a] Data from [23].

Table 6
Catalyst surface composition, binding energies for Mg 2p, C 1 s, Cs 3d and K 2p along with the Cu/Mg atomic ratio.

Catalyst	Composition (atomic%)						Cu/Mg (atom ratio)	Binding energy (eV)			
	C	O	Mg	Cu	K	Cs		Mg 2p	C 1s	Cs 3d	K 2p
0.5 wt% K–40 wt% Cu-MgO	26.5	40.2	31.5	1.9	–	–	0.06	50.86	285.88	–	–
0.5 wt% Cs–40 wt% Cu-MgO	23.6	39.3	35.5	1.6	–	–	0.04	50.84	285.92	–	–

Table 7
Binding energy value Cu $2p_{1/2}$, Cu $2p_{3/2}$ and Cu_s/Cu_p (area ratios of the Cu $2p_{3/2}$ (satellite) and Cu $2p_{3/2}$ (parent)).

Catalyst	Binding energy (eV)				Cu_s/Cu_p
	Cu $2p_{1/2}$ (satellite)	Cu $2p_{1/2}$ (parent)	Cu $2p_{3/2}$ (satellite)	Cu $2p_{3/2}$ (parent)	
CuO[a]	962.1	953.6	942.2	933.5	0.7164
Cu^0 [b]	–	952.5	–	932.7	–
0.5 wt% K–40 wt% Cu-MgO	963.5	953.6	943.2	933.8	0.2082
0.5 wt% Cs–40 wt% Cu-MgO	962.9	953.6	943.3	933.7	0.1504

[a] Data from [34].
[b] Data from previous study [38].

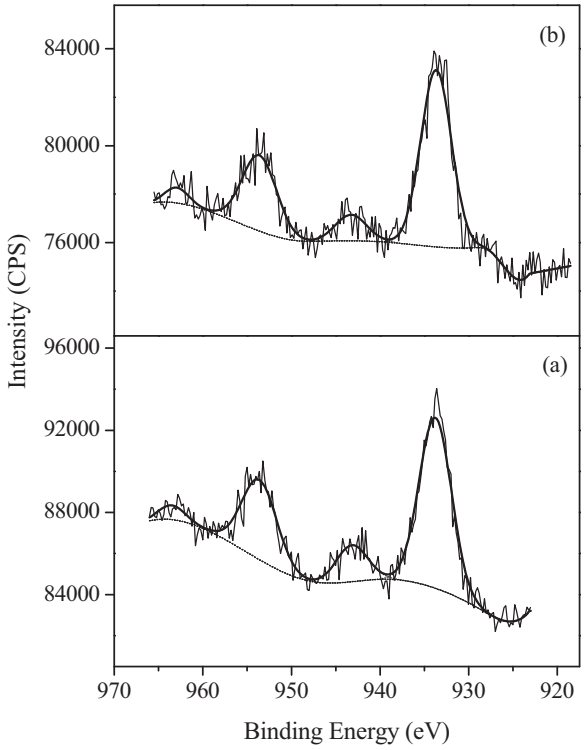

Fig. 5. Cu 2p XPS spectra for (a) 0.5 wt% K–40 wt% Cu-MgO, (b) 0.5 wt% Cs–40 wt% Cu-MgO.

(Table 7), which confirms the presence of Cu^0 in all the passivated K- or Cs-promoted-40 wt% Cu-MgO catalysts. The presence of CuO on the catalyst surface may be partly due to the fact that the K- or Cs-promoted-40 wt% Cu-MgO was passivated before XPS analysis. Hence the amount of Cu^0 on the catalyst surface estimated by XPS, represents the minimum amount of Cu^0 on the surface of the freshly reduced K- or Cs-promoted-40 wt% Cu-MgO present under reaction operating conditions.

3.2. Product distribution over MgO-based catalyst

Catalyst activity was determined for the 5 wt% Cu-MgO and the Cs– or K–5 wt% Cu-MgO at 101 kPa and 498K, with a feed composition of $He/CO/CH_3OH = 0.20/0.66/0.14$ (M) and a contact time (W/F) of 12.3×10^{-3} g min $(cm^3(STP))^{-1}$. A summary of the product distribution and the total net conversion of the reactants is given in Table 8. Over the 5 wt% Cu-MgO, the total net conversion was low (10.0 C-atom %) and methyl formate was the dominant product, whereas selectivity of CO_2 (S_{CO_2}) and C_2 species (S_{C_2}) was low (<6 C-atom%). Also, no CO was produced in the reaction. The total net conversion was increased as Cs or K was added to the 5 wt% Cu-MgO catalyst and the order of increase in the total net conversion was: 5 wt% Cu-MgO < 0.5 wt% K–5 wt% Cu-MgO < 0.5 wt% Cs–5 wt% Cu-MgO. Results of Table 8 showed that the selectivity to methyl formate (S_{MF}) at 498K increased in the order: 5 wt% Cu-MgO < 0.5 wt% K–5 wt% Cu-MgO < 0.5 wt% Cs–5 wt% Cu-MgO, whereas the reverse order was observed for S_{CO_2} and S_{C_2}. The trend observed for total net conversion, S_{MF} and S_{CO_2} are in good agreement with previous results reported for the 40 wt%

Table 8
Product distribution and catalyst activity over MgO-based catalysts.

Catalyst	W/F (min g(cm^{3}STP))$^{-1}$)	Reaction temperature (K)	Net CO consumption (C-atom %)	Net CH_3OH conversion (C-atom %)	Total net conversion[a] (C-atom %)	Product selectivity (C-atom %)			
						CO	MF[b]	CO_2	C_2[c]
40 wt% Cu-MgO[d]	12.3×10^{-3}	498	−9.7	84.7	75.0	68.4	29.3	1.5	0.9
0.5 wt% K–40 wt% Cu-MgO[d]	12.3×10^{-3}	498	−7.9	70.0	62.0	63.9	30.0	2.7	3.3
0.5 wt% Cs–40 wt% Cu-MgO[d]	1.3×10^{-3}	498	1.8	27.9	29.7	0.0	91.9	6.0	2.1
	12.3×10^{-3}	498	-6.1	66.7	60.6	53.4	34.9	8.4	3.4
5 wt% Cu-MgO	12.3×10^{-3}	498	3.3	6.6	10.0	0.0	92.5	5.2	2.3
	12.3×10^{-3}	523	4.2	12.5	16.7	0.0	95.4	2.4	2.2
0.5 wt% K–5 wt% Cu-MgO	12.3×10^{-3}	498	3.3	13.0	16.4	0.0	96.4	2.7	0.9
	12.3×10^{-3}	523	5.3	20.0	25.3	0.0	98.5	1.5	0.0
0.5 wt% Cs–5 wt% Cu-MgO	12.3×10^{-3}	498	7.8	26.4	34.2	0.0	98.0	1.5	0.5
	12.3×10^{-3}	523	9.3	34.6	43.9	0.0	98.8	1.0	0.2

Reaction conditions: 101 kPa, feed He/CO/CH_3OH = 0.20/0.66/0.14 molar, v_0 = 84.4 cm^3(STP) min^{-1}, for W/F = 12.3×10^{-3} min g(cm^3(STP))$^{-1}$ the catalyst weight is 0.98 g and for W/F = 1.3×10^{-3} min g(cm^3(STP))$^{-1}$ the catalyst weight is 0.1 g.

[a] Total conversion = net CO consumption + net CH_3OH conversion.
[b] MF stands for methyl formate.
[c] C_2 stands for C_2 species (ethanol and acetic acid).
[d] Experimental data were taken from the previous study [23].

Cu-MgO catalysts [23], whereas the trend observed for S_{C_2} is opposite to what was observed previously [23].

Over all of the 5 wt% Cu-MgO-based catalysts, an increase in operating temperature from 498 K to 523 K led to a small increase in S_{MF} and a small decrease in S_{CO_2} and S_{C_2} (Table 8), implying that an increase in operating temperature does not favour the C_2 species formation, as observed previously [23].

The total net conversion of the reactants decreased significantly for the Cu-MgO and alkali promoted Cu-MgO catalysts as the Cu loading decreased from 40 wt% to 5 wt%. The product distribution was also changed noticeably as a result of the change in the Cu loading and net conversions. Over the 40 wt% Cu-MgO-based catalysts at 498K and 12.3×10^{-3} min g(cm^3(STP))$^{-1}$, the selectivity to CO was highest among all the carbonaceous products whereas over the 5 wt% Cu-MgO-based catalysts at the same operating conditions, S_{CO} dropped to zero and selectivity to methyl formate was the highest among all the carbonaceous products.

4. Discussion

Over Cs- or K-promoted 5 wt% Cu-MgO-based catalysts, methyl formate was a dominant product (Table 8). Previously we demonstrated that on alkali promoted Cu-MgO, the product selectivity to methyl formate and C_2 was strongly influenced by the catalyst intrinsic basicity. Furthermore, it was noted that the presence of Cu on the surface of the Cs- or K-promoted Cu-MgO catalysts is important for the formation of methyl formate from CH_3OH/CO [23]. XPS studies suggested that the surface copper is present as Cu^{2+} and Cu^0 over Cs- or K-promoted Cu-MgO catalysts (Table 7). To investigate the effect of the Cu loading on methyl formate yield, the Cu^0 surface area (S_{Cu^0}) and Cu^{2+} surface area ($S_{Cu^{2+}}$) have been determined for the Cs- or K-promoted 5 wt% Cu-MgO catalysts and the Cs- or K-promoted 40 wt% Cu-MgO catalysts. These catalysts had similar intrinsic basicities (Table 5) so that differences in methyl formate yield must be due to differences in S_{Cu^0} and $S_{Cu^{2+}}$ and not due to differences in basicity. S_{Cu^0} was measured by N_2O chemisoption/decomposition. $S_{Cu^{2+}}$ for Cs- or K–40 wt% Cu-MgO was estimated as $S_{Cu^{2+}} = S_{Cu^{total}} - S_{Cu^0}$, where $S_{Cu^{total}}$ is the total copper surface area. To obtain an estimate of $S_{Cu^{total}}$ (Table 9) the Cu^{total}/Mg was obtained from the XPS analysis and we assumed that $S_{Cu^{total}} \cong S_{BET} \times (Cu^{total}/Mg)$. For the Cs- or K–5 wt% Cu-MgO, $S_{Cu^{2+}}$ could not be estimated in this way because as already discussed, the XPS analysis on K or Cs-promoted-5 wt% Cu-MgO catalysts showed no peak corresponding to Cu. However based on previously reported XPS studies on a 5.2 wt% Cu-MgO by Nagaraja et al. [34], who showed that Cu^{2+} was not detected on the catalyst surface, $S_{Cu^{2+}}$ was also assumed zero for the 5 wt% Cu-MgO catalysts in the present work. The methyl formate yield is plotted versus

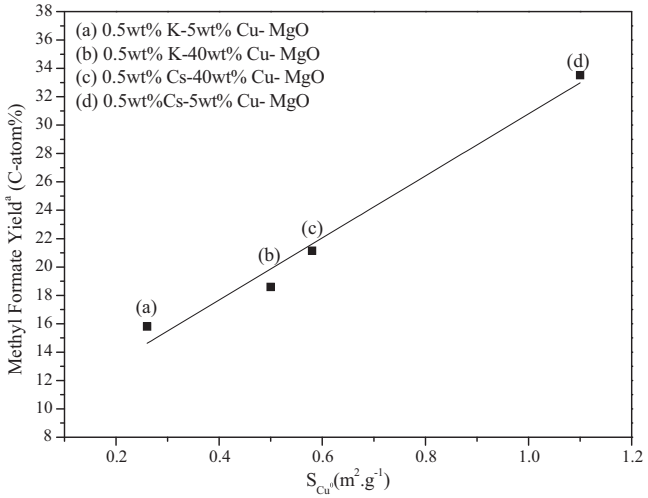

Fig. 6. Correlation between S_{Cu^0} and methyl formate yield.[a] Methyl formate yield is defined as the product of total net conversion and methyl formate selectivity.

Table 9
Cu^{2+} surface area and Cu^{total} surface area of Cu-MgO catalysts.

Catalyst	Cu^{total}/Mg (molar)[a]	$S_{Cu^{2+}}$ (m^2 g^{-1})	$S_{Cu^{total}}$ (m^2 g^{-1})
0.5 wt% K–40 wt% Cu-MgO	0.06	2.03[b]	2.53[b]
0.5 wt% Cs–40 wt% Cu-MgO	0.04	1.39[b]	1.97[b]
0.5 wt% K–5 wt% Cu-MgO	–	0.00[c]	0.26[c]
0.5 wt% Cs–5 wt% Cu-MgO	–	0.00[c]	1.10[c]

[a] Cu^{total}/Mg was measured based on XPS results.
[b] For Cu-MgO catalyst with Cu wt% = 40 wt%: $S_{Cu^{total}} = S_{BET} \times (Cu^{total}/Mg)$, $S_{Cu^{2+}} = S_{Cu^{total}} - S_{Cu^0}$
[c] For Cu-MgO catalyst with Cu wt% = 5 wt%: $S_{Cu^{2+}} = 0$ based on [34], $S_{Cu^{total}} = S_{Cu^{+2}} + S_{Cu^0} = S_{Cu^0}$.

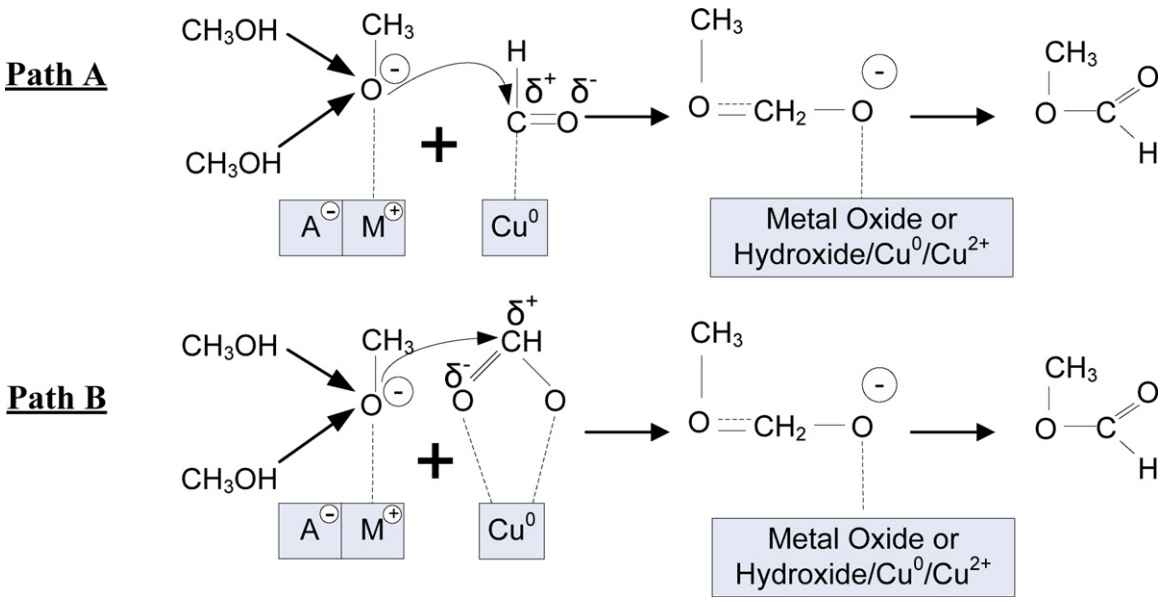

Fig. 7. Pathway for: (A) CH_3OH dimerization to methyl formate via methoxy and formyl intermediates, (B) CH_3OH dimerization to methyl formate via methoxy and formate intermediates. M^+ stands for Mg^{2+}, K^{1+} or Cs^{1+} and A^- stands for O^{2-} or OH^{-1}.

S_{Cu^0} (measured by N_2O adsorption) for the K- and Cs-promoted Cu-MgO catalysts in Fig. 6. The results show that an increase in S_{Cu^0} led to an increase in methyl formate yield. On the other hand no correlation between $S_{Cu^{2+}}$ and methyl formate yield was found. Over the 0.5 wt% K–5 wt% Cu-MgO and the 0.5 wt% Cs–5 wt% Cu-MgO catalyst, methyl formate was formed in the absence of Cu^{2+}. Based on these observations, it can be concluded that the formation of methyl formate was enhanced by Cu^0 (as opposed to Cu^{2+}).

Previously it was suggested that CH_3OH dimerization was a dominant pathway for the formation of methyl formate over Cu-MgO-based catalysts [23] and that methyl formate was formed by nucleophilic attack of a surface methoxy species on a surface formyl or formate species over the Cu-MgO-based catalysts [23,35,36]. IR studies suggest that the formation of formate species likely occurs on Cu sites over Cu–SiO_2 catalyst [26] and DFT studies suggest that formate species and formyl species can be formed on Cu sites of a Cu-ZnO catalyst [37]. On the other hand, based on in situ IR studies, formation of methoxy species was reported to take place on Cs^+ sites (basic site) on Cs–Cu-ZnO catalysts [13]. Based on these reports, we propose that over the Cu-MgO-based catalysts, methyl formate was formed by nucleophilic attack of a surface methoxy on a surface formyl or formate species. The methoxy species is adsorbed on basic sites (Mg^{2+}, K^+, Cs^+), and the formyl or formate is adsorbed on copper sites of the Cu-MgO catalysts [23,35,36]. Based on these mechanistic proposals and the observed effect of S_{Cu^0} on methyl formate yield, it can be concluded that surface formyl or formate species were most likely adsorbed on Cu^0 sites (as opposed to Cu^{2+} sites). The corresponding mechanism for CH_3OH dimerization to methyl formate is shown in Fig. 7. (Note that for simplicity, the hydrogenation–dehydrogenation steps are not shown in Fig. 7). It is important to note that based on DFT studies, it has been suggested that formyl species are not very stable on the Cu sites of Cu-ZnO catalysts and most likely dissociate to CO [37]. Consequently, path B of Fig. 7 may be considered the dominant pathway for the formation of methyl formate by CH_3OH dimerization on the alkali promoted Cu-MgO catalysts of the present work.

The data of Table 8 show that the CH_3OH conversion and product selectivity changed noticeably as the Cu loading decreased from 40 wt% to 5 wt% in the Cs- or K-promoted Cu-MgO (Table 8). The changes in selectivity could be due to the fact that the conversion decreased noticeably as a result of a decrease in the Cu loading. In order to investigate the effect of Cu loading on the formation mechanism of the different carbonaceous products (mainly methyl formate and C_2 species) over Cs- or K-promoted Cu-MgO, the product selectivity over the Cs- or K-promoted 5 wt% Cu-MgO and the Cs- or K-promoted 40 wt% Cu-MgO should be compared at the same conversion. Such data are summarized in Table 8. Comparing the product distribution over the 0.5 wt% Cs–40 wt% Cu-MgO at $W/F = 1.3 \times 10^{-3}$ min g $(cm^3(STP))^{-1}$ and a total net conversion of 29.7%, with the 0.5 wt% Cs–5 wt% Cu-MgO at $W/F = 12.3 \times 10^{-3}$ min g $(cm^3(STP))^{-1}$ and a total net conversion of 34.2%, shows relatively the same product distribution over both catalysts. A decrease in Cu loading from 40 wt% to 5 wt% in the 0.5 wt% Cs–Cu-MgO catalyst, did not affect the product distribution noticeably at the same conversion. Furthermore, it can be concluded that the corresponding mechanisms for the formation of methyl formate and C_2 species from CH_3OH and CO over the 5 wt% Cu-MgO-based catalyst and the 40 wt% Cu-MgO-based catalysts are the same.

5. Conclusion

Cu-MgO, 0.5 wt% K–Cu-MgO and 0.5 wt% Cs–Cu-MgO with 5 wt% Cu loading were prepared by thermal decomposition of the metal salts in the presence of palmitic acid. The results of catalytic tests over the catalysts at 101 kPa, 498 K and $W/F = 12.3 \times 10^{-3}$ min g $(cm^3(STP))^{-1}$ with a CO/He/CH_3OH (0.20/0.66/0.14) feed gas, showed that in all cases, methyl formate was the dominant product. It was found that the corresponding mechanisms for the formation of methyl formate and C_2 species from CH_3OH and CO over the 5 wt% Cu-MgO-based catalyst and the 40 wt% Cu-MgO-based catalysts were the same. For the 5 wt% Cu-MgO-based catalysts and the 40 wt% Cu-MgO-based catalysts, the correlation between the S_{Cu^0} and methyl formate yield at approximately constant specific basicity (384.5–415.9 μmol CO_2 g^{-1}) showed that an increase in S_{Cu^0} led to an increase to methyl formate yield, whereas no correlation between $S_{Cu^{2+}}$ and methyl formate yield were observed, suggesting that formation of methyl formate was enhanced by the presence of Cu^0 sites as opposed to Cu^{2+} sites.

Acknowledgement

Financial support from Natural Science and Engineering Research Council (NSERC) of Canada is gratefully acknowledged.

References

[1] A. Walter, F. Rosillo-Calle, P.B. Dolzan, E. Piacente, K. Borges da Cunha, Unicamp, IEA Bioenergy, 2007, p. 41.
[2] J.R. Rostrup-Nielsen, Science 308 (2005) 1421.
[3] V. Subramani, S.K. Gangwal, Energy Fuels 22 (2008) 814.
[4] K. Klier, V. Chatikavanij, R.G. Herman, G.W. Sim, J. Catal. 74 (1982) 343.
[5] K. Klier, Adv. Catal. 31 (1982) 243.
[6] J.C.J. Bart, R.P.A. Sneeden, Catal. Today 2 (1987) 1.
[7] G.W. Bridger, M.S. Spencer, Catalyst Hand book, second ed., Wolfe Publ. Co, London, 1989.
[8] R.G. Herman, New Trends in CO Activation, Amsterdam, Elsevier, 1991.
[9] J.R. LeBlanc, R.V. Schneider III, R.B. Strait, Methanol Production and Use, Marcel Dekker, New York, 1994.
[10] P.B. Rasmussen, P.M. Holmbald, T. Askgaard, C.V. Ovesen, P. Stoltze, J.K. Norskov, I. Chorkendorff, Catal. Lett. 26 (1994) 373.
[11] G.C. Chinchen, P.J. Denny, J.R. Jennings, M.S. Spencer, K.C. Waugh, Appl. Catal. 36 (1987) 1.
[12] Y.F. Zhao, Y. Yang, C. Mims, C.H.F. Peden, J. Li, D. Mei, J. Catal. 281 (2011) 199.
[13] J.G. Nunan, C.E. Bogdan, K. Klier, K.J. Smith, C.W. Young, R.G. Herman, J. Catal. 113 (1988) 410.
[14] J.G. Nunan, C.E. Bogdan, R.G. Herman, K. Klier, Catal. Lett. 2 (1989) 49.
[15] J.G. Nunan, C.E. Bogdan, K. Klier, K.J. Smith, J. Catal. 116 (1989) 195.
[16] G.A. Vedage, P.B. Himelfarb, G.W. Simmons, K. Klier, Am. Chem. Soc. Symp. Ser. 279 (1985) 295.
[17] T.S. Askgaard, J.K. Norskov, C.V. Ovesen, P. Stoltze, J. Catal. 156 (1995) 229.
[18] D.B. Clarke, A.T. Bell, J. Catal. 154 (1995) 314.
[19] S. Fujita, M. Usui, H. Ito, N. Takezawa, J. Catal. 157 (1995) 403.
[20] M. Xu, E. Iglesia, Catal. Lett. 51 (1988) 47.
[21] M. Xu, E. Iglesia, J. Catal. 188 (1999) 125.
[22] J. Nunan, K. Klier, C.W. Young, P.B. Himelfarb, R.G. Herman, J. Chem. Soc. Chem. Commun. 193 (1986) 193.
[23] S. Goodarznia, K.J. Smith, J. Mol. Catal. A: Chem. 320 (2010) 1.
[24] F. Arena, G. Italiano, K. Barbera, S. Bordiga, G. Bonura, L. Spadaro, F. Frusteri, Appl. Catal. A 350 (2008) 16.
[25] W. Cheng, H.H. Kung, Methanol Production and Use, first ed., Marcel Dekker, New York, 1994.
[26] Y. Yang, C.A. Mims, R.S. Disselkamp, D. Mei, J.H. Kwak, J. Szanyi, C.H.F. Peden, C.T. Campbell, Catal. Lett. 125 (3–4) (2008) 201.
[27] S. Sato, M. Iijima, T. Nakayama, T. Sodesawa, F. Nozaki, J. Catal. 169 (1997) 447.
[28] S. Takenaka, R. Takahashi, T. Sodesawa, Phys. Chem. Chem. Phys. 5 (2003) 4968.
[29] N. Lopez, F. Illas, J. Phys. Chem. 100 (1996) 16275.
[30] Y. Inoue, I. Yasumori, Bull. Chem. Soc. Jpn. 54 (1981) 1505.
[31] H. Onishi, C. Egawa, T. Aruga, Y. Iwasawa, Surf. Sci. 191 (1987) 479.
[32] S.F. Zaman, K.J. Smith, Appl. Catal. A: Gen. 378 (2010) 59.
[33] S.J. Yang, C.W. Bates, Appl. Phys. Lett. 36 (1980) 675.
[34] B.M. Nagaraja, A.H. Padmasri, B. David Raju, K.S. Rama Rao, J. Mol. Catal. A: Chem. 265 (2007) 90.
[35] L. Domokos, T. Katona, A. Molnar, Catal. Lett. 40 (1996) 215.
[36] M.J. Chung, D.J. Moon, K.Y. Park, S.K. Ihm, J. Catal. 136 (1992) 609.
[37] Y. Yang, J. Evans, J.A. Rodriguez, M.G. White, P. Liu, Phys. Chem. Chem. Phys. 12 (2010) 9909.
[38] R.J. Bird, P. Swift, J. Electron Spectrosc. Relat. Phenom. 21 (1980) 227.